Spectra and correlated wave functions of two electrons confined in a quasi-one-dimensional nanostructure

Tokuei Sako*
Laboratory of Physics, College of Science and Technology, Nihon University, 7-24-1 Narashinodai, Funabashi, 274-8501 Chiba, Japan

Geerd H. F. Diercksen†
Max-Planck-Institut für Astrophysik, Karl-Schwrzschild-Strasse 1, D-85741 Garching, Germany
(Received 20 November 2006; published 14 March 2007)

The energy spectra and wave functions of two electrons confined by a quasi-one-dimensional Gaussian potential have been calculated for different strengths of confinement, ω_z, and anharmonicity by using the quantum chemical full configuration interaction method employing a Cartesian anisotropic Gaussian basis set. The energy spectra for a nearly harmonic Gaussian potential have been studied and analyzed in three regimes of ω_z: namely, large (ω_z=5.0), medium (ω_z=1.0), and small (ω_z=0.1). For large and medium ω_z the energy spectrum shows a band structure which is characterized by the polyad quantum number v_p while for small ω_z it is characterized by the *extended* polyad quantum number v_p^*. The energy levels for small ω_z form doublet pairs each of which consists of a pair of singlet and triplet states. The nodal patterns of their wave functions are almost identical to each other except for their phases. The energy spectra for the strongly anharmonic Gaussian potential look quite similar to those of the nearly harmonic case except that an irregular level structure appears in the high-energy region for ω_z=0.1. The wave functions of the states in this high-energy region have curved *nodal lines* which align along a pair of bent *nodal coordinates*. Two types of pairs of bent nodal coordinates have been identified: namely, those passing through the valley of the confining potential and the others passing on the hillside. It is shown that the wave functions with these nodal coordinates correspond to new types of classical *local-mode* motions of electrons.

DOI: 10.1103/PhysRevB.75.115413 PACS number(s): 73.21.La, 68.65.Hb, 71.10.Li, 71.15.Ap

I. INTRODUCTION

Recent developments of semiconductor technology allow the construction of nanostructures on semiconductor surfaces[1–3] and have triggered theoretical studies on quantum systems consisting of a small number of electrons confined in such engineered nanospaces.[4] Because of their finite size, these quantum systems have a discrete energy-level structure that follows Hund's rules[5,6] well known for atoms. Therefore they are referred to as artificial atoms or quantum dots.

One of the most significant differences between quantum dots and atoms is that the electronic properties of quantum dots can be controlled by the size of the dots—namely, the strength of confinement,[7] as well as by the shape[8,9] and by the dimensionality.[10,11] Because of this property, quantum dots are regarded as potential sources for lasers[12,13] and quantum computers.[14,15] Indeed, it has been demonstrated computationally that the energy-level structure of quantum dots changes strongly for different strengths of confinement.[4,16–20] For the strong limit the confining potential dominates the energy spectrum and the electron-electron interaction plays only a minor role. On the other hand, as the strength of confinement decreases the electron-electron interaction starts to affect the energy spectrum more and more strongly and the energy-level structure gets complicated.[4] At the weak limit of confinement the electron correlation becomes so large that it breaks the shell structure resulting from the confining potential.[20,21] For practical applications of quantum dots as future quantum devices the relation between the form of the confining potential, the resultant energy spectra, and the dynamics of the electrons needs to be well established.

In the present study, as a first step toward this goal, quantum dots have been modeled by two interacting electrons confined in a quasi-one-dimensional Gaussian potential.[22,23] This model allows the wave functions of the electrons to be visualized in a two-dimensional plane and permits a detailed analysis of the correlation of the confined electrons. A Gaussian potential has been chosen as confining potential that is approximated in the low-energy region by a harmonic-oscillator potential typically used for modeling semiconductor quantum dots.[4,17,24] Introducing anharmonicity into the confining potential is important for simulating realistic confining potentials[25] as well as for studying the breakdown of the generalized Kohn theorem.[24,26–31] The eigenvalues and wave functions of the two electrons confined in the quasi-one-dimensional Gaussian potential have been calculated by using the quantum chemical full configuration interaction (CI) method employing a Cartesian anisotropic Gaussian basis set with large angular momentum functions.[32] The computed energy spectra and wave functions have been examined by focusing on the nodal pattern in the CI wave functions. Atomic units are used throughout this paper.

II. COMPUTATIONAL METHODOLOGY

A. Theoretical model

The Hamiltonian operator adopted in the present study is given by

$$\mathcal{H} = \sum_{i=1}^{2} \left[-\frac{1}{2}\nabla_i^2 \right] + \sum_{i=1}^{2} w(\mathbf{r}_i) + \frac{1}{|\mathbf{r}_1 - \mathbf{r}_2|}, \quad (1)$$

where the one-electron confining potential $w(\boldsymbol{r})$ is chosen to be the sum of an isotropic harmonic-oscillator potential for the x and y directions and an attractive Gaussian-type potential for the z direction and is given by

$$w(\boldsymbol{r}) = \frac{1}{2}\omega_{xy}{}^2[x^2 + y^2] - D \exp\left[-\frac{\omega_z^2}{2D} z^2 \right]. \quad (2)$$

For a sufficiently large value of ω_{xy} the electrons bound by the potential of Eq. (2) are strongly compressed along the x and y directions and have degrees of freedom only along the z direction. Therefore the system can be regarded as a quantum system confined by a quasi-one-dimensional Gaussian potential. The value of ω_{xy} in Eq. (2) is set to 20 a.u. for all calculations in the present study. The computed spectra do not strongly depend on this value unless the energy gets close to or larger than ω_{xy}. Since the Gaussian potential of Eq. (2) can be approximated close to the minimum by a harmonic-oscillator potential with the confinement strength of ω_z, the above potential is suitable for modeling the confining potential of semiconductor quantum dots with anharmonicity.[33]

The anharmonicity of the Gaussian potential in Eq. (2) can be characterized as defined in a previous study[32] by the ratio of the confinement strength ω_z over the depth of the Gaussian potential D as

$$\alpha = \omega_z/D. \quad (3)$$

By using this anharmonicity parameter the studied system can be described by two parameters: namely, by the strength of confinement ω_z and by α.

The total energies and wave functions of the electrons confined by the quasi-one-dimensional Gaussian potential of Eq. (2) have been calculated as the eigenvalues and eigenvectors of the full CI matrix. All calculations have been performed by using OpenMol,[34] which has been extended to account for Gaussian and power-series potentials and *anisotropic* Gaussian basis functions.[32] The results are presented in atomic units and can be scaled by the effective Bohr radius of 9.79 nm and the effective Hartree energy of 11.9 meV for GaAs semiconductor quantum dots.[35,36]

B. Basis set

In previous studies of this series[18,19,32,37] it has been demonstrated that a set of properly chosen Cartesian *anisotropic* Gaussian-type orbitals (c-aniGTO's) is the most convenient choice to correctly approximate the wave function of electrons confined in anisotropic potentials. A c-aniGTO basis set can be transformed into a set of eigenfunctions of the corresponding three-dimensional anisotropic harmonic oscillator.[19] Therefore it would be useful also for calculating with high accuracy eigenvalues and eigenfunctions of atoms in strong magnetic fields[38–41] and of semiconductor quantum dots.[42,43] In the present study a c-aniGTO basis set has been placed at the center of the confining potential:—i.e., at the origin of the Cartesian coordinate system. The orbital exponents for the x and y directions have been chosen as $\omega_{xy}/2$ while that for the z direction accounting for the Gaussian potential in Eq. (2) has been determined in the same way as described in a previous study.[32] Since ω_{xy} is much larger than ω_z, those functions that have nodal lines only along the z direction *without* nodal lines along the x and y directions have been selected and used in the basis sets.[20,32]

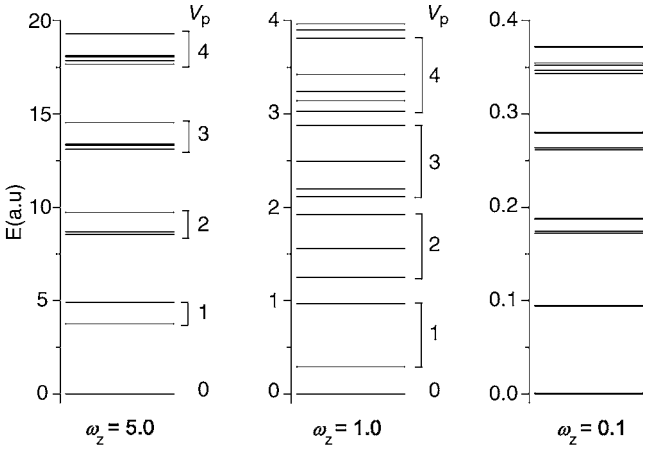

FIG. 1. Energy spectrum of two electrons confined by a quasi-one-dimensional Gaussian potential with different strengths of confinement, ω_z, represented as relative energies from the ground state. The anharmonicity parameter α of the Gaussian potential is 0.05 for all cases. The vertical axis of each of the three energy diagrams is scaled by ω_z so that the energy of the ground state and the excitation energy of four quanta of ω_z are at the same level of the vertical axis, respectively.

In order to check the reliability of the c-aniGTO basis set with respect to calculating the energy spectra of two-electrons confined by the potential of Eq. (2) the convergence of the resultant energies calculated by increasing the size of the basis set has been examined for the Gaussian potentials with $(D, \omega_z) = (2.0, 0.1)$ and (0.8, 0.1). The number of basis functions was increased stepwise by adding a new function with an additional nodal line to the previous basis set. The maximum deviation of the energy levels covered by the present study was shown to be smaller than 2×10^{-4} for the results obtained by using basis sets with 13 and 14 functions, respectively, whose highest-angular-momentum function has 12 and 13 nodal lines, respectively. For the rest of the study the basis set of 13 functions has been used.

III. RESULTS AND DISCUSSION

A. Nearly harmonic case

The energy spectra of two electrons confined by the quasi-one-dimensional Gaussian potentials with $(D, \omega_z) = (100.0, 5.0)$, (20.0, 1.0), and (2.0, 0.1) have been calculated and are displayed in Fig. 1. The anharmonicity parameter α defined by Eq. (3) has been chosen as 0.05 for all cases which corresponds to a relatively harmonic shape of the Gaussian potential. The vertical axis of each of the three energy diagrams is scaled by ω_z so that the energy of the

ground state and the excitation energy of four quanta of ω_z are at the same level of the vertical axis, respectively. Therefore, *if* there is no electron-electron interaction, all three energy spectra will look identical in this representation. On the other hand, as shown in Fig. 1, the energy-level structure changes drastically for different strength of ω_z, indicating that the effect of electron-electron interaction on the spectrum changes strongly for different ω_z.

The energy spectrum for $\omega_z=5.0$ displayed on the left-hand side of Fig. 1 shows a band structure in which energy levels having the same *polyad quantum number* lie close to each other while those with different values of v_p are well separated from each other. The polyad quantum number was introduced in a previous study[32] and specifies in the present model the total number of nodes in the leading configuration of the CI wave functions. By using the polyad quantum number the energy-level structure for $\omega_z=5.0$ is interpreted as follows: In the strong limit of confinement the effect of electron-electron interactions becomes negligibly small and the energy spectrum is completely dominated by the confining potential. For a harmonic confining potential the energy levels with the same polyad quantum number $v_p=q$ form in the strong limit a group of $(q+1)$-fold degenerate levels. For example, the polyad manifold of $v_p=2$ consists of three states, two from the configuration $0^1 2^1$ (singlet and triplet) and one from the configuration 1^2 (singlet), in which the numbers m and n in the notation m^n represent the one-electron harmonic-oscillator quantum number m and its occupation number n in the configuration, respectively. As the strength of confinement ω_z decreases from the strong limit the electron-electron interaction starts to affect the spectrum by splitting the degenerate levels within each of the polyad manifolds as observed for $\omega_z=5.0$

As ω_z decreases the splitting of levels within polyad manifolds becomes larger and energy levels belonging to adjacent polyad manifolds come close to each other as observed in the spectrum for $\omega_z=1.0$ displayed in the middle of Fig. 1. For the range of $\omega_z \geqslant 1.0$ the energy spectrum can be interpreted by using the polyad quantum number v_p since different polyad manifolds are energetically separated. When ω_z decreases further energy levels belonging to different polyad manifolds start to overlap with each other. In the small limit of ω_z energy levels belonging to different polyads for large ω_z interact with each other through the electron-electron interaction and form a new structure of energy levels. Since the polyad quantum number is an approximately conserved quantity, the overlap of energy levels having different polyad quantum numbers may lead to lowering this constant of motion and in turn give rise to *quantum chaotic states* as known for vibrationally highly excited states of small polyatomic molecules.[44,45]

The results for $\omega_z=0.1$ displayed on the right-hand side of Fig. 1 show, however, that the energy level structure is not irregular as observed for chaotic vibrational spectra but quite regular with a similar band structure as observed for ω_z of 5.0. It is noted that the energy spectrum for $\omega_z=0.1$ differs from that of $\omega_z=0.5$ in that all levels form nearly degenerate *doublets* each of which consists of a pair of singlet and triplet states belonging to different polyad manifolds for large ω_z. For example, the energy levels at $E=0.095$, 0.188, and 0.280, each of which looks like a single level in Fig. 1, are doubly degenerate, respectively, as well as the apparent doublets at $E=0.173$ and 0.263. A similar doublet structure was reported previously for two electrons confined in a quasi-one-dimensional rectangular potential well of large size[16,46] as a precursor of the Wigner lattice.[47] Therefore, the observed doublet energy-level structure can be a general trend for weakly confined two-electron systems. It is also noted that the number of levels belonging to each band is counted from the lowest band as 2, 2, 4, 4, and 6 for $\omega_z=0.1$ while the corresponding number is 1, 2, 3, 4, and 5, respectively, for $\omega_z=5.0$ and 1.0.

In order to understand the origin of the doublet structure observed in the energy spectrum for $\omega_z=0.1$ in Fig. 1 the energy levels for $\omega_z=1.0$, 0.5, and 0.1 and the square density of the corresponding wave functions are displayed in Fig. 2. The vertical axis of each of the three energy-level diagrams is scaled by ω_z so that the excitation energy of one quantum of ω_z is at the same level of the vertical axis. The electronic wave functions are plotted as the square density in the two electron coordinates z_1 and z_2 by integrating over the remaining four spatial coordinates of x_1, x_2, y_1, and y_2 and over the spin coordinates, respectively. The square density distribution of the wave functions in the z_1-z_2 plane is simply called wave function hereafter.

For $\omega_z=1.0$ the assignment ${}^{2S+1}[n_s,n_a]$ of the wave functions has been made by using the spin multiplicity $2S+1$ and by the pair of numbers n_s and n_a counting the number of *nodal lines* along the *symmetric coordinate* z_s and the *antisymmetric coordinat* z_a, respectively, which are defined by

$$z_s = \frac{1}{\sqrt{2}}[z_1 + z_2], \tag{4}$$

$$z_a = \frac{1}{\sqrt{2}}[z_1 - z_2]. \tag{5}$$

The nodal lines of a wave function are defined by the lines along which the density of the wave function is exactly zero. The symmetric coordinate z_s and antisymmetric coordinate z_a coincide with the 45° diagonal line and with the other diagonal line in the density plots, respectively. For example, in the case of $\omega_z=1.0$ the wave function of the seventh excited ${}^3[2,1]$ state has two nodal lines along the symmetric coordinate and one nodal line along the antisymmetric coordinate while the eighth excited ${}^1[1,2]$ state has one nodal line along the symmetric coordinate and two nodal lines along the antisymmetric coordinate. It is noted that the spin multiplicity—i.e., singlet or triplet—can be derived also from the density plots in Fig. 2. According to the Pauli principle the spatial part of the wave function must be either symmetric or antisymmetric with respect to the exchange of the coordinates z_1 and z_2 and the symmetric and antisymmetric wave functions have to be coupled to the singlet and triplet spin functions, respectively. The symmetric wave functions do not change their sign with respect to a reflection about the symmetric coordinate while the antisymmetric wave functions change their sign. Although the phase information is not displayed in the density plots in Fig. 2, wave

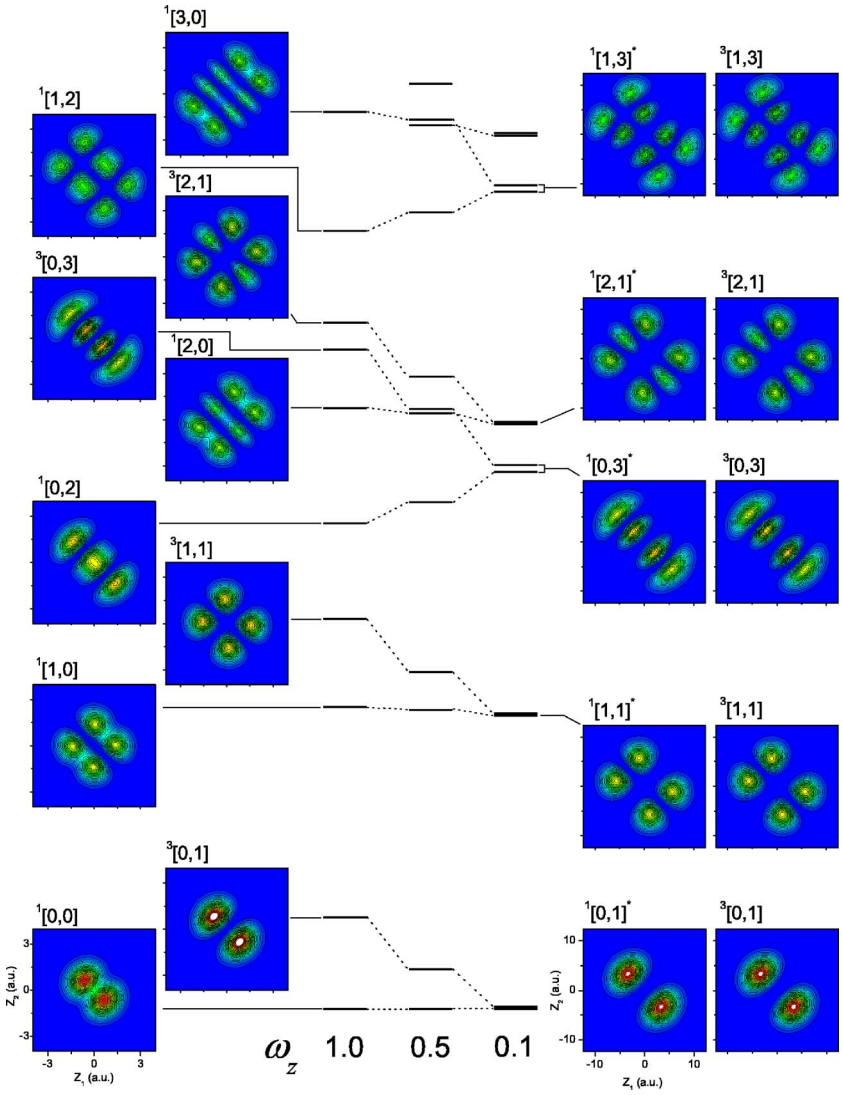

FIG. 2. (Color online) Correspondence of the low-lying energy levels and wave functions of two electrons confined in a quasi-one-dimensional Gaussian potential. The anharmonicity parameter α of the Gaussian potential is 0.05 for all cases. The vertical axis of each of the three energy diagrams is scaled by ω_z so that the excitation energy of one quantum of ω_z is on the same level. The electronic wave functions are plotted as the square density in the two electron coordinates z_1 and z_2. The assignment of wave functions has been made by counting the number of nodal lines along the symmetric and antisymmetric electron coordinates for $\omega_z=1.0$ while an *extended* assignment marked by an asterisk has been made for the singlet wave functions with $\omega_z=0.1$ (see text).

functions must change their sign in passing through a nodal line. Therefore, those wave functions which have *symmetric coordinate as a nodal line* are antisymmetric wave functions while the others are symmetric wave functions. In the above example the wave function of the $^3[2,1]$ state has a nodal line that coincides with the symmetric coordinate. Therefore, this wave function is of opposite sign in the two regions separated by the symmetric coordinate and must be coupled to the triplet spin function. On the other hand, the wave function of the $^1[1,2]$ state does not have a nodal line that coincides with the symmetric coordinate. Therefore, this wave function does not change sign with respect to a reflection about the symmetric coordinate and must be coupled to the singlet spin function.

As shown in Fig. 2 the energy levels of the lowest singlet $^1[0,0]$ state and the lowest triplet $^3[0,1]$ state become nearly degenerate as ω_z decreases from 1.0 to 0.1. Moreover, the wave function of the singlet $^1[0,0]$ state, which has no nodal line for $\omega_z=1.0$, apparently has a diagonal nodal line that coincides with the symmetric coordinate and has a nodal pattern very similar to that of the triplet $^3[0,1]$ state for $\omega_z=0.1$. It is noted that the wave function of the $^1[0,0]$ state has the same sign on both sides of the symmetric coordinate since it is a singlet state. Therefore, in a strict sense the symmetric coordinate of the wave function of the lowest singlet $^1[0,0]$ state for $\omega_z=0.1$ is not a nodal line. However, since the density of the wave function along the symmetric coordinate is negligibly small, it is convenient to regard the symmetric coordinate in this case as a nodal line in assigning the nodal pattern. Therefore the assignments of the singlet wave functions for $\omega_z=0.1$ in Fig. 2 marked with an asterisk are *extended* assignments in which the symmetric coordinate with negligible density is included in counting the number of nodal lines along the antisymmetric coordinate. By using this convention the assignments for the lowest doublets are $^3[0,1]^*$ and $^3[0,1]$, respectively, which clearly supports the observation that the spatial distributions of the singlet and triplet wave functions are quite similar to each other but differ in their phases.

A similar observation can be made for the second lowest doublet in Fig. 2. The pair of the states $^1[1,0]$ and $^3[1,1]$ in this doublet have a different number of nodal lines and are energetically separated for $\omega_z=1.0$. As ω_z decreases these two levels come closer to each other, and at $\omega_z=0.1$ they form a nearly degenerate doublet. The corresponding wave

functions for $\omega_z=0.1$ have quite similar nodal patterns but differ in their phases such that the singlet wave function is symmetric about the symmetric coordinate while the triplet wave function is antisymmetric with respect to it.

Another interesting observation concerning the second lowest doublet is the relative insensitivity of the energy level of the singlet $^1[1,0]$ state with respect to the change of ω_z compared to the strong decrease of the energy of the triplet $^3[1,1]$ state as ω_z decreases from 1.0 to 0.1. The insensitivity of the singlet $^1[1,0]$ state is interpreted as a consequence of the *generalized Kohn theorem*. The excitation energy of the dipole-allowed transitions which correspond to an excitation into the *center-of-mass* mode is according to this theorem for harmonic potentials always equal to ω_z irrespective of the effect of the electron-electron interaction. In the present case the $^1[1,0]$ state in the second doublet is dipole allowed from the lowest $^1[0,0]$ state since the wave function of this state has one additional nodal line along the symmetric coordinate as compared to the lowest $^1[0,0]$ state. Since according to the definition of Eq. (4) the symmetric coordinate is proportional to the *center-of-mass coordinate* of $\frac{1}{2}[z_1+z_2]$, the additional nodal line along the symmetric coordinate indicates an excitation of one quantum into the center-of-mass mode. The energy-level diagrams in Fig. 2 have been scaled so that the excitation energy of one quantum of ω_z is at the same level for different values of ω_z. Therefore the excitation energy of the dipole-allowed transition from the lowest state should be in the harmonic limit of the confining potential at the same height for the energy-level diagrams with different values of ω_z. The weak ω_z dependence of the energy level of the $^1[1,0]$ state represented in Fig. 2 is due to the small anharmonicity of the Gaussian potential.

Similar observations can be made for the fourth doublet consisting of the $^1[2,0]-^3[2,1]$ pair of states. The singlet $^1[2,0]$ state is relatively insensitive to the change of ω_z as previously observed for the $^1[1,0]$ state in the second doublet. Although this singlet $^1[2,0]$ state is not dipole allowed from the lowest $^1[0,0]$ state, it is dipole allowed from the $^1[1,0]$ state in the second doublet. Therefore, since the energy level of the $^1[1,0]$ state is relatively insensitive to the change of ω_z as discussed in the last paragraph, the energy level of the $^1[2,0]$ state is also only weakly dependent on ω_z. On the other hand, in the case of the third doublet consisting of the $^1[2,0]-^3[0,3]$ pair of states the energy levels of the triplet state *and* the singlet state change strongly as ω_z decreases. This strong ω_z dependence of the singlet energy level can be understood also by the nodal pattern in the wave function. As displayed in Fig. 2 the wave function of the singlet $^1[0,2]$ state has no nodal line along the symmetric coordinate, indicating that the $^1[0,2]$ state is not dipole allowed from any lower-lying states. Therefore, the generalized Kohn theorem does not apply to this case.

The above observations and their interpretation based on an examination of the nodal pattern of the wave functions and the correspondence of the energy levels for different values of ω_z can be summarized as follows: For $\omega_z \geqslant 1.0$ the energy levels can be grouped into sets with respect to their polyad quantum number v_p. The singlet $^1[n_s,n_a]$ states and the triplet $^3[n_s,n_a+1]$ states are energetically separated since they belong to different polyad manifolds with $v_p=n_s+n_a$ and n_s+n_a+1, respectively. As ω_z decreases the density along the symmetric coordinate in the singlet wave functions decreases and eventually it becomes a nodal line in the sense of the extended assignment defined above. For $\omega_z=0.1$ the singlet state has the same number of nodal lines as the triplet state using the extended assignment and they form a nearly degenerate doublet.

In order to understand the origin of the appearance of the new nodal line in the singlet wave functions for small ω, the sum of the one- and two-electron potential functions in the Hamiltonian of Eq. (1) projected onto the z_1-z_2 plane,

$$V(z_1,z_2)=\sum_{i=1}^{2} D\left[1-\exp\left(-\frac{\omega_z^2}{2D}z_i^2\right)\right]+\frac{1}{|z_1-z_2|}, \qquad (6)$$

has been calculated and displayed in Fig. 3 for $(D,\omega_z)=(100.0,5.0)$, (20.0, 1.0), and (2.0, 0.1), respectively, where the minimum of the one-electron potential has been chosen as the reference point of energy.

In all three cases displayed in Fig. 3 the maximum potential height is $10\omega_z$ and the domain of the coordinates z_1 and z_2 is chosen such that for the one-dimensional harmonic-oscillator potentials the classical turning points for the energy value of $10\omega_z$ coincide with the limits of the domain. In this representation the energy contours for the one-electron part of the potential—i.e., the first-term on the right-hand side of Eq. (6)—are identical for different values of ω_z. Therefore, differences in the contours among different ω_z must be ascribed to the electron-electron interaction potential. As shown in Figs. 3(a)–3(c) the diagonal line separating the contours into two regions that represents the potential wall of the electron-electron interaction becomes thicker as ω_z decreases from 5.0 to 0.1. This indicates that the wave functions bound in this potential are influenced by the electron-electron interaction potential more strongly for smaller ω_z.

Based on the contour plots of the potential function $V(z_1,z_2)$ the ω_z dependence of the energy spectra and the wave functions displayed in Figs. 1 and 2, respectively, can be interpreted as follows: As shown in Fig. 3(a) the potential wall of the electron-electron interaction for $\omega_z=5.0$ is so thin that the electron-electron interaction acts only as a perturbation to the potential function $V(z_1,z_2)$ which is dominated by the one-electron confining potential. Since a set of energy levels belonging to the same polyad manifold are nearly degenerate if there is no electron-electron interaction as explained above, the splitting of the nearly degenerate energy levels observed for $\omega_z=5.0$ is due to *tunneling* through the thin potential wall. The level ordering after the splitting may be explained by the relative amount of density of the wave functions along this potential wall. For example, the energy eigenstates belonging to the polyad manifold of $v_p=2$ are $^3[1,1]$, $^1[0,2]$, and $^1[2,0]$ in increasing order of their energy. The wave functions of these three states are displayed in Fig. 4 for $\omega_z=5.0$ and 1.0 in the same way as in Fig. 2. Only the triplet $^3[1,1]$ state has a nodal line that coincides with the symmetric coordinate: namely, along the potential wall as observed in Fig. 4. The energy increase due to the potential

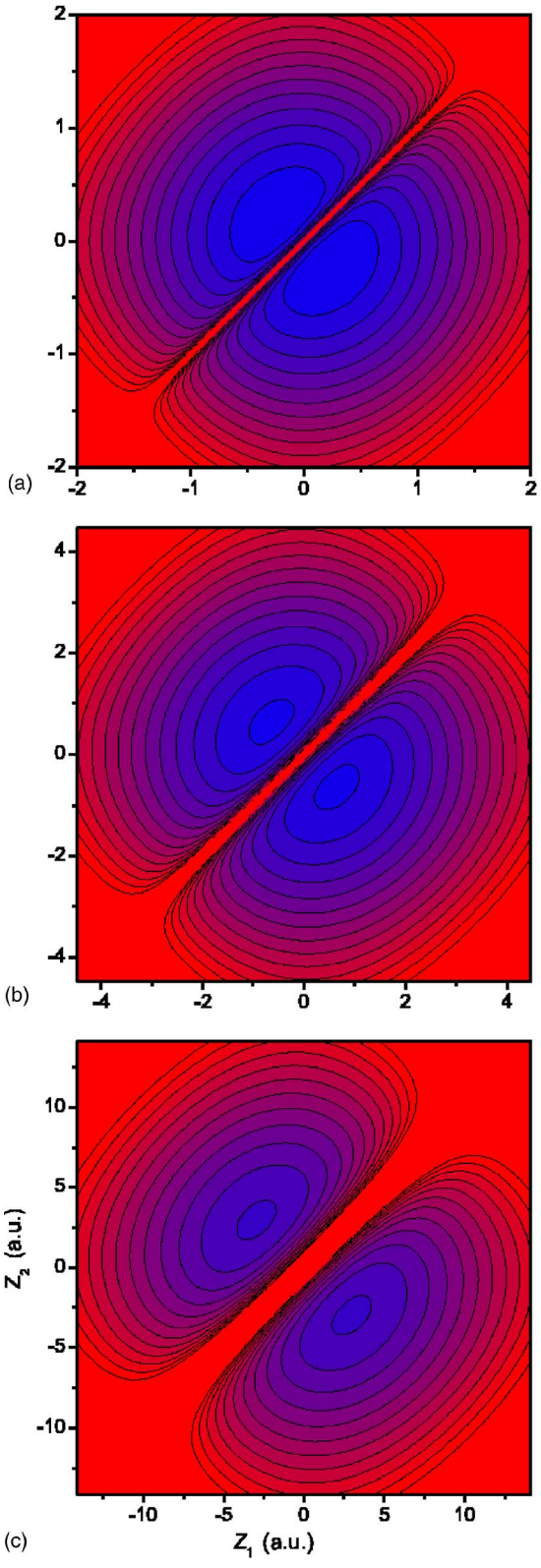

FIG. 3. (Color online) Two-dimensional contour plot of the sum of the Gaussian and of the electron repulsion potentials for ω_z =5.0 (a), 1.0 (b), and 0.1 (c). The anharmonicity parameter for the Gaussian potential and the maximum potential height displayed are 0.05 and 10 ω_z, respectively, for all cases. The diagonal line separating the contours into two regions represents the potential wall of the electron repulsion potential.

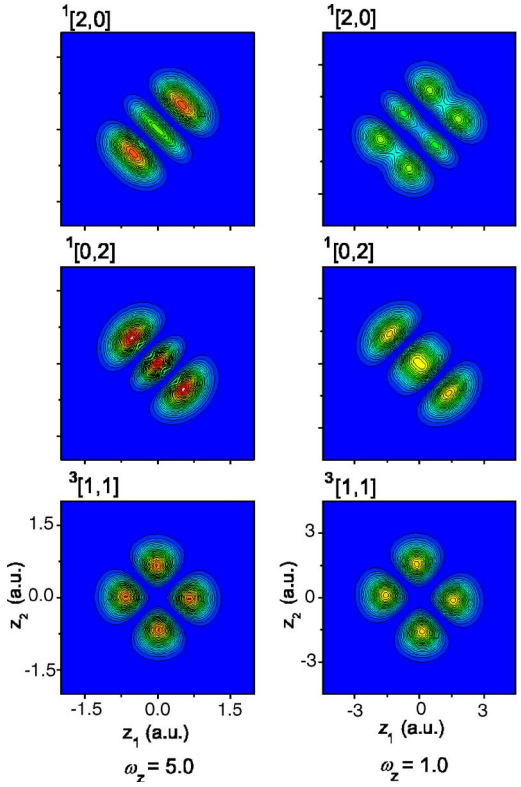

FIG. 4. (Color online) Square density plot of the wave functions for the three states in the polyad manifold of v_p=2 of two electrons confined in a quasi-one-dimensional Gaussian potential with ω_z =5.0 and 1.0. The anharmonicity parameter α of the Gaussian potential is 0.05.

wall may be estimated by integrating the density $\rho(z_1,z_2)$ multiplied by the electron-electron interaction potential over a region close to the potential wall:

$$\Delta E_{wall} = \int_{\Omega} \rho(z_1,z_2) \frac{1}{|z_1 - z_2|} dz_1 dz_2, \tag{7}$$

where Ω denotes a domain of integration close to the potential wall. Because of the existence of a nodal line along the potential wall for the triplet state, the energy increase ΔE_{wall} for the triplet state is much smaller than that for the singlet states. In case of the two singlet states the wave function of the $^1[0,2]$ state extends along the antisymmetric coordinate while that of the $^1[2,0]$ state extends along the symmetric coordinate as displayed on the left-hand side of Fig. 4. Therefore, ΔE_{wall} is larger for the $^1[2,0]$ state than for the $^1[0,2]$ state since the density in the domain of integration Ω is larger for $^1[2,0]$ than for $^1[0,2]$. This suggests that the energy of the $^1[2,0]$ state is larger than that of the $^1[0,2]$ state in accordance with the observed energy-level ordering.

As ω_z decreases from 5.0 to 1.0 the potential wall of the electron-electron interaction becomes wider as shown in Fig. 3(b). Consequently, the magnitude of the splitting due to tunneling becomes larger and for ω_z=1.0 it becomes comparable to ω_z as observed for the corresponding spectrum in Fig. 1. The effect of the increase in the width of the potential

wall is most clearly visible for the wave function of the $^1[2,0]$ state. As shown in Fig. 4 for $\omega_z=5.0$ the wave function of the $^1[2,0]$ state has the peak of the density distribution along the symmetric coordinate—i.e., along the potential wall-while for $\omega_z=1.0$ it has the peak shifted towards both sides of the potential wall, resulting in a smaller increase of ΔE_{wall}. The reduction of density along the potential wall in the singlet wave functions may rationalize the well-known observation that electron correlation or configuration mixing is larger for a singlet wave function than for the corresponding triplet wave function of the same configuration.[20,21] As noted, the triplet wave functions originally have a nodal line along the potential wall while the singlet wave functions do not. Therefore, as ω_z decreases the singlet states require stronger configuration interactions in order to "create" a dent of density in the wave functions along the potential wall.

As displayed in Fig. 3(c) for $\omega_z=0.1$ the width of the potential wall is so thick that the electron-electron interaction potential is no more a perturbation to $V(z_1,z_2)$. Therefore it is better to adopt a zeroth-order picture in which the wave functions bound to either of the two spatial regions separated by the potential wall interact with each other weakly. By transforming the coordinates from (z_1,z_2) to (z_s,z_a) and introducing a harmonic approximation to the Gaussian potential in Eq. (6) the zeroth-order Hamiltonian for the upper (+) and lower (−) bound regions separated by the potential wall in Fig. 3(c) can be approximated by

$$\mathcal{H}^{\pm}_{\omega_z=0.1}=h_s+h^{\pm}_a, \tag{8}$$

where h_s and $h^{\pm}_a$ are defined, respectively, by

$$h_s=-\frac{1}{2}\frac{\partial^2}{\partial z_s^2}+\frac{1}{2}\omega_z^2 z_s^2, \tag{9}$$

$$h^{\pm}_a=-\frac{1}{2}\frac{\partial^2}{\partial z_a^2}+\frac{1}{2}\omega_z^2 z_a^2, \tag{10}$$

where the domain of the antisymmetric coordinate z_a in Eq. (10) is defined by $z_a<0$ for h^+_a and $z_a>0$ for h^-_a. In the approximation made above the Coulomb tail of the potential wall is neglected. The Hamiltonian h_s of Eq. (9) is that of a harmonic oscillator with ω_z and with the eigenvalue given by $\epsilon_s(v_s)=\omega_z(v_s+\frac{1}{2})$ for $v_s=0,1,2,\ldots$. The Hamiltonian $h^{\pm}_a$ is also that of a harmonic oscillator but it is defined in the domain $z_a>0$ or $z_a<0$, and its wave functions are zero at $z_a=0$ because of the existence of the huge potential wall. It is noted that the standing waves that are bound in a harmonic-oscillator potential and vanish at the origin are the eigenfunctions of this harmonic oscillator with *odd* quantum numbers defined either in the positive or in the negative domain of z_a. The eigenvalues of the Hamiltonian (10) are therefore given by $\epsilon^{\pm}_a(v_a)=\omega_z(v_a+\frac{1}{2})$ for $v_a=1,3,5,\ldots$. Consequently, the eigenvalues for the zeroth order Hamiltonian (8) are determined by

TABLE I. Zeroth-order energy levels $E^{\pm}$ for $\omega_z=0.1$ defined by Eq. (11).

v_s	v_a	v_p^{*a}	$E^{\pm}/\omega_z$
0	1	1	2
1	1	2	3
0	3	3	4
2	1	3	4
1	3	4	5
3	1	4	5
0	5	5	6
2	3	5	6
4	1	5	6

[a]The *extended* polyad quantum number.

$$E^{\pm}(v_s,v_a)=\omega_z[v_s+v_a+1], \tag{11}$$

where $v_s=0,1,2,\ldots$ and $v_a=1,3,5,\ldots$. It is noted that E^+ and E^- have the same energy spectrum.

By using the energy formula of Eq. (11) the origin of the characteristic features of the energy-level structure for $\omega_z=0.1$—that is, the regular band structure consisting of doublets as represented in Figs. 1 and 2—can be rationalized as follows: For $\omega_z=0.1$ the electron-electron interaction results in a strong potential wall. Therefore the interaction between the zeroth-order levels E^+ and E^- is very small and only pairs of energy levels having the same energy can interact to some extent with each other. This results in the formation of doublets consisting of an in-phase superposition state (singlet) and an out-phase superposition state (triplet). Their energies are almost identical to those of the zeroth-order levels with a small splitting due to tunneling. Therefore, the energy spectrum for $\omega_z=0.1$ is basically the same as the spectrum of the zeroth-order levels given by Eq. (11) within the harmonic approximation except that each level is doubly degenerate. The low-lying energy levels of Eq. (11) are listed in Table I together with the *extended* polyad quantum number v_p^* defined by the sum of v_s and v_a. The extended polyad quantum number specifies the number of nodal lines in the wave functions for $\omega_z=0.1$ displayed in Fig. 2. As shown in Table I the lowest energy level has the assignment $(v_s,v_a)=(0,1)$ which is not the usual harmonic-oscillator ground state $(v_s,v_a)=(0,0)$ since v_a starts from 1 by the definition. This level forms the lowest doublet consisting of the $^1[0,1]^*$ and $^3[0,1]$ states displayed in Fig. 2. The second lowest level has the assignment $(v_s,v_a)=(1,1)$, which forms the eigenstates $^1[1,1]^*$ and $^3[1,1]$. As shown in Table I the energy of this second lowest level is one quantum of ω_z larger than that of the lowest level. This is consistent with the observation that the energy difference between the lowest $^1[0,1]^*$ state and the second lowest singlet $^1[1,1]^*$ state is close to ω_z as a consequence of the generalized Kohn theorem. The third and fourth lowest levels with $(v_s,v_a)=(0,3)$ and (2, 1), respectively, have the same v_p^* of 3 and the same energy of $4\omega_z$. This is again one quantum of ω_z larger than that of the second level. The corresponding doublets have the eigenstates

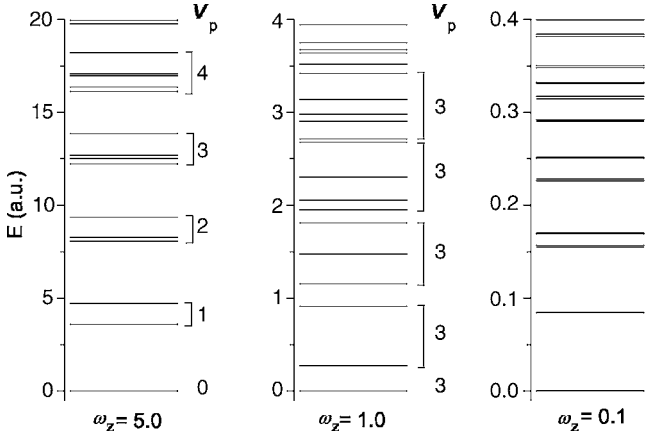

FIG. 5. Excitation energy spectrum of two electrons confined in a quasi-one-dimensional Gaussian potential with different strengths of confinement, ω_z. The anharmonicity of the Gaussian potential α is 0.125 for all cases. The vertical axis of each of the three energy diagrams is scaled by ω_z so that the energy of the ground state and the excitation energy of four quanta of ω_z are at the same level of the vertical axis, respectively.

$^1[0,3]^* - ^3[0,3]$ and $^1[2,1]^* - ^3[2,1]$, respectively. Their energies are roughly one ω_z larger than the energies of the second doublet. By repeating this procedure it can be understood that the zeroth-order energy spectrum of Eq. (11) has a band structure characterized by v_p^* with a band-gap energy of ω_z and that the number of levels belonging to the v_p^* manifold is $(v_p^*+1)/2$ for odd v_p^* and $v_p^*/2$ for even v_p^*. Therefore, the regular band structure of the energy spectrum for $\omega_z=0.1$ can be ascribed to the harmonic energy spectrum of Eq. (11). The degeneracy pattern of it accounts for the number of energy levels that belong to each of the bands specified by v_p^*: that is, v_p^*+1 for odd v_p^* and v_p^* for even v_p^*.

B. Anharmonic case

The energy spectra of two electrons confined by the quasi-one-dimensional Gaussian potential with $(D,\omega_z)=(40.0,5.0)$, (8.0, 1.0), and (0.8, 0.1) have been calculated and are displayed in Fig. 5 in the same way as in Fig. 1. The anharmonicity parameter α is 0.125 for all cases and corresponds to a Gaussian potential with relatively large anharmonicity. This value has been chosen such that all energy levels located in the energy range covered by the present study—that is, $4\omega_z$ from the lowest state—are below the first ionization limit.[32] When α becomes larger than this value some energy levels close to the upper limit of the energy range become unbound.

The energy spectra for $\omega_z=5.0$ and 1.0 displayed in Fig. 5 show a band structure very similar to that of the corresponding spectra in Fig. 1 and are characterzied by the polyad quantum number v_p. The energy differences between adjacent polyad manifolds are slightly smaller for the spectra shown in Fig. 5 than for those in Fig. 1. This is due to the larger anharmonicity of the Gaussian potential of the spectra displayed in Fig. 5. On the other hand, in case of the spectrum for $\omega_z=0.1$ a significant difference is observed in the higher-energy region above $E=0.3$ between the results displayed in Figs. 1 and 5. In the lower energy region both energy spectra in Figs. 1 and 5 for $\omega_z=0.1$ have a band structure which can be correlated with each other up to the fourth lowest band: namely, the band with $v_p^*=4$. For the higher-lying energy levels such a correspondence is obviously not clear. Indeed, the energy levels in the higher energy region displayed in Fig. 5 do not form a band structure with a band gap of ω_z as observed in Fig. 1 but a rather irregular level structure. Since the regular band structure for the nearly harmonic case with an energy gap of ω_z is due to the harmonic energy spectrum of the zeroth-order levels given by Eq. (11), the irregular level structure in the higher-energy region observed in Fig. 5 is due to the effect of the large anharmonicity.

In order to understand the irregular energy-level structure in the energy spectrum for $\omega_z=0.1$ observed in Fig. 5 the square density of their wave functions is displayed in Fig. 6 in the same way as in Fig. 2. The assignment of the wave functions has been made by counting the number of nodal lines along the symmetric and antisymmetric coordinates. For the singlet wave functions the symmetric coordinate is treated as a nodal line in determining n_a; that is, the extended assignment has been adopted as in Fig. 2.

The wave functions of the lowest and second lowest doublets displayed in Fig. 6 show nodal patterns quite similar to those of the corresponding wave functions in Fig. 2. On the other hand, in the case of the third doublet consisting of the $^1[0,3]^*$ and $^3[0,3]$ states the outer rims of the wave functions extend into a much larger spatial region than those of the corresponding wave functions in Fig. 2. A similar observation is made for the wave functions of the $^1[1,3]^*$ and $^3[1,3]$ states in the fifth doublet, which are dipole allowed from the $^1[0,3]^*$ and the $^3[0,3]$ state, respectively. It is noted that most of the nodal lines in the wave functions above the second doublet in Fig. 6 are not straight lines as observed in Fig. 2 but are curved more and more strongly, indicating an increasingly stronger mixing of the two degrees of freedom z_s and z_a through anharmonicity. Nevertheless, the wave functions can still be assigned up to the six lowest doublets by counting the number of the curved nodal lines along the symmetric and the antisymmetric coordinates.

In the case of seventh and tenth doublets consisting of the $^1[2,3]^*$ and $^3[2,3]$ states and the $^1[1,5]^*$ and $^3[1,5]$ states, respectively, on the other hand, the nodal lines are so strongly curved that it is apparently not clear how many nodal lines should be counted along the symmetric and antisymmetric coordinates. A similar difficulty occurs for the eighth and ninth doublets but by an analogy to the nodal pattern of the pair of wave functions located in a lower-energy region—namely, of the $^1[0,3]^*$ and $^3[0,3]$ states and of the $^3[3,1]^*$ and $^3[3,1]$ states, respectively—they can be assigned as $^1[0,5]^*$ and $^3[0,5]$ states and as $^1[4,1]^*$ and $^3[4,1]$ states, respectively. By assuming that the seventh doublet originally belongs to the polyad manifold of $v_p^*=5$ for smaller anharmonicity its states have been assigned tentatively as the remaining possibility in this manifold: namely, to the $^1[2,3]^*$ and $^3[2,3]$ states, as shown in Table I. The assignment of the $^1[1,5]^*$ and $^3[1,5]$ states of the tenth dou-

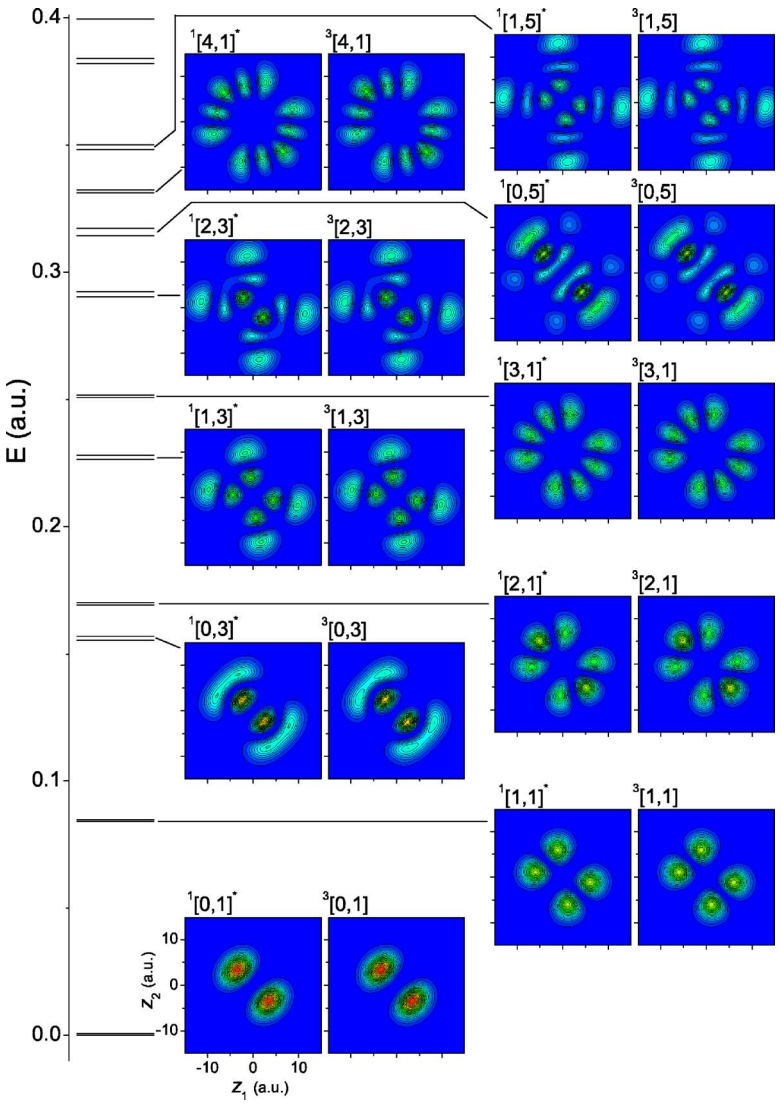

FIG. 6. (Color online) Square density plot of the wave functions for the low-lying states of two electrons confined in a quasi-one-dimensional Gaussian potential with $(D,\omega_z)=(0.8,0.1)$. The assignment of wave functions has been made by counting the number of nodal lines along the symmetric and antisymmetric electron coordinates. The assignment marked by an asterisk given to the singlet wave functions is the *extended* assignment (see text).

blet has been made in a similar way by assuming that it belongs to the $v_p^*=6$ manifold for smaller anharmonicity.

C. Local-mode wave functions

The characteristic nodal pattern observed in the wave functions of the seventh and tenth doublets, consisting of the $^1[2,3]^*$ and $^3[2,3]$ states and of the $^1[1,5]^*$ and $^3[1,5]$ states respectively, displayed in Fig. 6 looks similar to that of the *local-made vibratinal wave function* of the stretching vibrations of *ABA* molecules,[48] such as H_2O (Ref 49) and SO_2 in the vibrationally highly excited states.[50–53] It is known in molecular vibrational spectroscopy that the two *A*-*B* stretching vibrations in an *ABA* molecule that form the symmetric and antisymmetric stretching normal-mode vibrations become decoupled from each other to form doubly degenerate local-mode vibrations when the anharmonicity in the potential energy surface dominates the momentum coupling between the two *A*-*B* stretching vibrations.[54] The resulting doubly degenerate local-mode vibrational wave functions correspond to the two semiclassical trajectories in which one *A*-*B* bond vibrates strongly while the other stays in a zero-point vibration.[49,52]

The correspondence between the classical trajectories and vibrational wave functions representing the local-mode vibrations can be most clearly observed by forming the sum and the difference of the doubly degenerate vibrational wave functions.[48,50] The resulting wave functions have only nodal lines along one stretching coordinate and no nodal lines along the other stretching coordinate, indicating that one stretching vibration is highly excited while the other stays in its ground state. In order to understand the dynamics of the two electrons in the $^1[1,5]^*$ and $^3[1,5]$ doublet states the sum and difference of the wave functions of the corresponding states are displayed in Fig. 7 in the same way as for Figs. 2 and 6. The nodal lines of the wave functions shown in Figs. 7(c) and 7(d) do not align parallel to either of the electron coordinates as for the local-mode vibrational wave functions but align along a bent coordinate, indicating that these wave functions represent a different electron motion than the local-mode vibrations. This kind of a curved coordinate along which nodal lines align may be an example of the *nodal coordinate*[55] proposed in analyzing vibrational wave functions of vibrationally highly excited states of polyatomic molecules.[44] By recalling that a distribution of wave func-

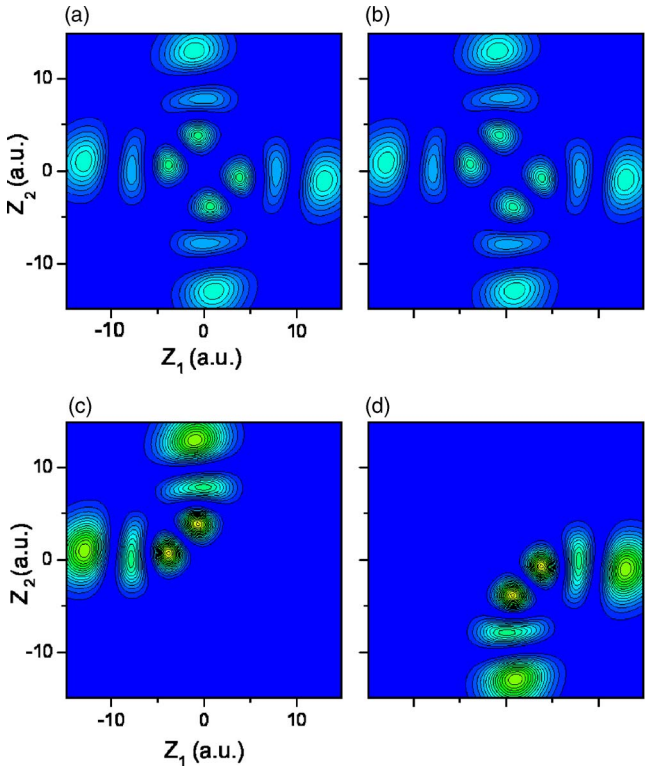

FIG. 7. (Color online) Square density plot of the wave functions for the doublet pair $^1[1,5]^*$ (a) and $^3[1,5]$ (b) and their sum (c) and difference (d).

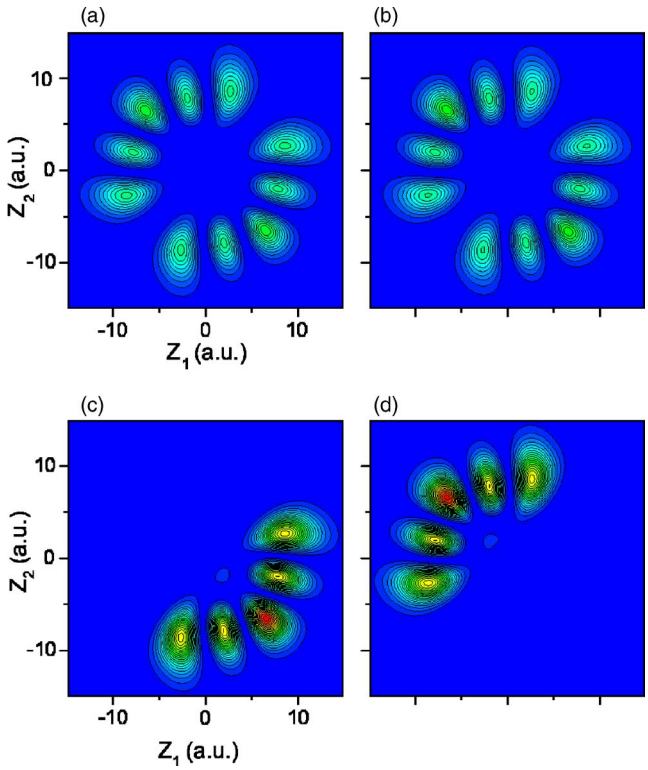

FIG. 8. (Color online) Square density plot of the wave functions for the doublet pair $^1[4,1]^*$ (a) and $^3[4,1]$ (b) and their sum (c) and difference (d).

tions can be interpreted as a torus of classical periodic orbits, the wave functions in Figs. 7(c) and 7(d) can be interpreted as follows: The distribution of the wave function (c) extends along the line of $z_2=0$ for $z_1<0$ and along the line of $z_1=0$ for $z_2>0$. In the part of the wave function extending along $z_2=0$, only electron 1 moves in the range of $-15<z_1<0$ while electron 2 stays close to the origin of the coordinate. On the other hand, in the part of the wave function extending along $z_1=0$, only electron 2 moves in the range of $0<z_2<15$ while electron 1 stays close to the origin. Therefore, the wave function (c) corresponds to a two-body elastic collision of identical particles in classical mechanics in which electron 1 approaching from the negative z direction collides with electron 2 at the origin and transfers its momentum to it. Then electron 2 starts moving along the positive z direction while electron 1 stays at the origin. The wave function in Fig. 7(d) corresponds to the classical motion obtained by inverting that of the wave function in Fig. 7(c) with respect to the origin of the coordinates: that is, electron 2 coming from the negative z direction collides with electron 1 at the origin and so on. This analysis shows that the wave functions of the tenth doublet in Fig. 6 represent a different type of localized electron modes than the well-known local mode in molecular vibrations, although their nodal patterns resemble each other.

It is instructive to apply a similar analysis to the wave functions of the states of the ninth doublet in Fig. 6 which have a characteristic nodal pattern different from the previous case. The sum and difference of the wave functions of the two states $^1[4,1]^*$ and $^3[4,1]$ forming ninth doublet are displayed in Figs. 8(c) and 8(d), respectively, in the same way as in Fig. 7. As observed in Figs. 8(c) and 8(d) the nodal coordinates of these wave functions are bent as in the case of the wave functions of the tenth doublet in Figs. 7(c) and 7(d) but they are located in different spatial regions as compared to those of the tenth doublet. The distribution of the wave function in Fig. 8(c) extends along $-3<z_1<8$ for $z_2=-8$ and along $-8<z_2<3$ for $z_1=8$. Therefore, in classical mechanical interpretation electron 1 moves in the positive direction from $z_1=-3$ to 8 while electron 2 stays at $z_2=-8$. Then electron 2 starts to move towards the same direction from $z_2=-8$ to 3 while the electron 1 stays at $z_1=8$. This indicates that electron 2 follows the movement of electron 1 after a quarter cycle of one oscillation. Therefore, the wave functions of the ninth doublet, again, show another type of localized electron modes different from the local mode in molecular vibration.

In order to understand the origin of these two new types of localized electron modes observed in the ninth and tenth doublets the sum of the one- and two-electron potential functions, $V(z_1,z_2)$ in Eq. (6), projected onto the z_1-z_2 plane has been calculated and displayed in Fig. 9 for $(D,\omega_z)=(0.8,0.1)$. The maximum potential height and the range of the coordinates z_1 and z_2 are the same as in Fig. 3(c). It is seen in Fig. 9 that the valley of the potential—i.e., the minimum-energy path from the bottom of the potential—extends along two bent lines indicated schematically by the dotted lines and arrows. Such a valley is not observed in Fig. 3(c) for the nearly harmonic case. This means that for the strongly anharmonic potential of Fig. 9 the wave functions of electrons bound in this potential prefer a nodal pattern ex-

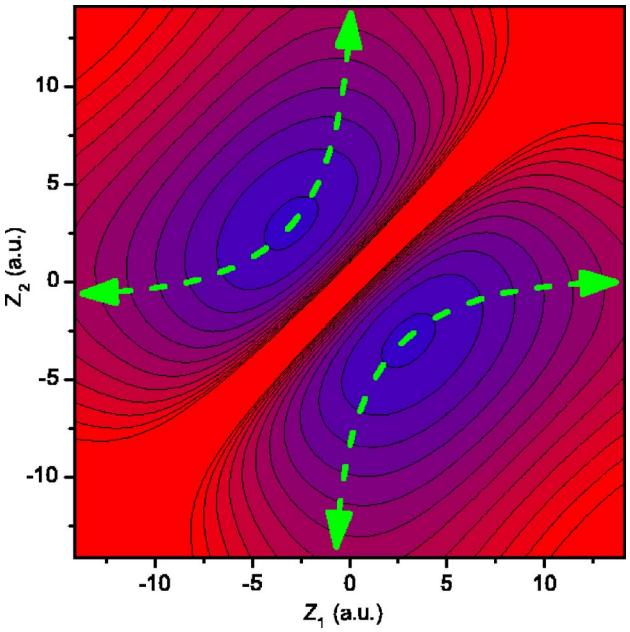

FIG. 9. (Color online) Two-dimensional contour plot of the sum of the Gaussian and of the electron-repulsion potentials for $(D,\omega)=(0.8,0.1)$. The maximum potential height displayed and the range of the coordinates z_1 and z_2 are the same as in Fig. 3(c). The lines allows represent the valleys of the potential.

tending along these two bend lines. The wave functions of the $^1[2,3]^*$ and $^3[2,3]$ states and the $^1[1,5]^*$ and $^3[1,5]$ states, respectively, belonging to the seventh and tenth doublets in Fig. 6, are of this type. On the other hand, the wave functions of the $^1[4,1]^*$ and $^3[4,1]$ states forming the ninth doublet do not extends along a valley but on the hillside of the potential. Therefore, these wave functions may correspond to a pair of unstable classical periodic orbits. In both cases the wave functions tend to have nodal lines not along the coordinates of the correlated motion of two electrons, z_s and z_a, but along the coordinates local to each electron: namely, z_1 and z_2.

IV. SUMMARY

In the present study the energy spectra and wave functions of two electrons confined by a quasi-one-dimensional Gaussian potential have been calculated for different strengths of confinement and anharmonicity by using the quantum chemical configuration interaction method employing reduced Cartesian anisotropic Gaussian basis sets. The most important results of the study are summarized as follows.

The energy spectra for a nearly harmonic Gaussian potential have been calculated, analyzed, and classified for three regimes of confinement strength ω_z: namely, strong ($\omega_z=5.0$), medium ($\omega_z=1.0$), and weak ($\omega_z=0.1$) confinement. For the strong confinement the energy spectrum shows a regular band structure with a band gap close to ω_z. The energy levels of each band are well localized and are characterized by the *polyad quantum number* v_p defined as the sum of the nodal lines n_s and n_a of the wave functions along the symmetric and the antisymmetric coordinate, respectively. The number of energy levels belonging to each band is equal to v_p+1. For medium confinement the energy spectrum shows also a band structure characterized by v_p but the splitting of the energy levels belonging to the same v_p manifold is so large that adjacent polyad manifolds get close to each other. As the confinement becomes even weaker energy levels belonging to different v_p manifolds start to overlap with each other. For the small confinement strength of $\omega_z=0.1$ the triplet energy levels having the set of nodal lines (n_s,n_a) for $n_s=0,1,2,\ldots$ and $n_a=1,3,5,\ldots$, respectively, become nearly degenerate with the singlet energy levels that have the nodal lines (n_s,n_a-1) for strong and medium confinement. By introducing an extended assignment for the singlet wave function in which the symmetric coordinate is treated as a nodal line in determining n_a the singlet and triplet wave functions in the degenerate pair have the same set of nodal lines (n_s,n_a). The energy spectrum of the weak confinement has a band structure with a band-gap of about ω_z as observed for the strong confinement but each band is characterized by the *extended* polyad quantum number v_p^*. The number of levels belonging to the v_p^* manifold is shown to be v_p^*+1 for odd v_p^* and v_p^* for even v_p^*.

The square density of the wave functions for the nearly harmonic case has been plotted in the two-dimensional z_1-z_2 plane, and its nodal pattern has been examined. It has been shown that the density of the singlet wave functions along the symmetric coordinate becomes smaller as ω_z decreases and that it becomes negligibly small for $\omega_z=0.1$. The singlet wave functions at $\omega_z=0.1$ have the same number of nodal lines as their counterpart triplet wave functions of the degenerate pairs using the extended assignment. Their nodal patterns become almost identical to each other except for their phases. The sum of the one- and two-electron potentials projected onto the z_1-z_2 plane $V(z_1,z_2)$ shows that the decreasing density along the symmetric coordinate in the singlet wave functions for decreasing ω_z is caused by the increasingly stronger potential wall of the electron-electron interaction along this coordinate.

The energy spectra for a strongly anharmonic Gaussian potential have been calculated, analyzed, and classified for the same three regimes of confinement strength ω_z as for the nearly harmonic case. For the strong and medium confinement the energy spectra look quite similar to those of the nearly harmonic case. But for weak confinement of $\omega_z=0.1$ the spectrum shows an irregular level structure in the high energy region above $E\geqslant 0.3$. The nodal lines of the wave functions in this high-energy region get increasingly curved as the energy increases, and it becomes more and more difficult to assign these wave functions by counting the number of nodal lines along the symmetric and antisymmetric coordinates. By taking the sum and the difference of the singlet and triplet wave functions of the degenerate pairs two types of a pair of bent *nodal coordinates*, along which the nodal pattern of the wave functions extend, have been identified: namely, one pair of coordinates passing through the valley of the potential $V(z_1,z_2)$ and the other pair passing on the hillside. It is shown that the wave functions having the nodal coordinates through the valley correspond to a classical mo-

tion of two electrons performing an elastic collision and that those having the nodal lines on the hillside correspond to a classical motion in which one electron follows the movement of the other electron after a quarter cycle. Both of these localized electron motions have resulted as a consequence of large anharmonicity in the confining potential.

ACKNOWLEDGMENTS

The present study has been supported in part by the Grants-in-Aid for Scientific Research (No. 18750018) from the Ministry of Education, Science, Sports and Culture and by the fund from the Matsuo Foundation. T.S. thanks the Alexander von Humboldt Foundation for support.

*Electronic address: sako@phys.ge.cst.nihon-u.ac.jp; URL: http://www.phys.ge.cst.nihon-u.ac.jp/~sako/

†Electronic address: ghd@mpa-garching.mpg.de; URL: http://www.mpa-garching.mpg.de/mol_physics/index.shtml

[1] C. B. Murray, D. J. Norris, and M. G. Bawendi, J. Am. Chem. Soc. **115**, 8706 (1993).
[2] R. C. Ashoori, Nature (London) **379**, 413 (1996).
[3] S. Tarucha, D. G. Austing, T. Honda, R. J. van der Hage, and L. P. Kouwenhoven, Phys. Rev. Lett. **77**, 3613 (1996).
[4] N. F. Johnson, J. Phys.: Condens. Matter **7**, 965 (1995).
[5] L. Kouwenhoven, T. H. Oosterkamp, M. W. S. Danoesastro, M. Eto, D. G. Austing, T. Honda, and S. Tarucha, Science **278**, 1788 (1997).
[6] P. Matagne, J. P. Leburton, D. G. Austing, and S. Tarucha, Physica E (Amsterdam) **13**, 679 (2002).
[7] A. P. Alivisatos, Science **271**, 933 (1996).
[8] T. Ezaki, N. Mori, and C. Hamaguchi, Phys. Rev. B **56**, 6428 (1997).
[9] G. Cantele, D. Ninno, and G. Iadonisi, Phys. Rev. B **64**, 125325 (2001).
[10] J. Hu, T. W. Odom, and C. M. Lieber, Acc. Chem. Res. **32**, 435 (1999).
[11] M. Rontani, F. Rossi, F. Manghi, and E. Molinari, Phys. Rev. B **59**, 10165 (1999).
[12] V. I. Klimov, A. A. Mikhailovsky, S. Xu, A. Malko, J. A. Hollingsworth, C. A. Leatherdale, H.-J. Eisler, and M. G. Bawendi, Science **290**, 314 (1996).
[13] L. Pavesi, L. D. Negro, C. Mazzoleni, G. Franzó, and F. Priolo, Nature (London) **408**, 440 (2000).
[14] E. Biolatti, R. C. Iotti, P. Zanardi, and F. Rossi, Phys. Rev. Lett. **85**, 5647 (2000).
[15] D. Loss and D. P. DiVincenzo, Phys. Rev. A **57**, 120 (1998).
[16] G. W. Bryant, Phys. Rev. Lett. **59**, 1140 (1987).
[17] U. Merkt, J. Huser, and M. Wagner, Phys. Rev. B **43**, 7320 (1991).
[18] T. Sako and G. H. F. Diercksen, J. Phys. B **36**, 1433 (2003).
[19] T. Sako and G. H. F. Diercksen, J. Phys.: Condens. Matter **15**, 5487 (2003).
[20] T. Sako and G. H. F. Diercksen, J. Phys.: Condens. Matter **17**, 5159 (2005).
[21] B. Szafran, J. Adamowski, and S. Bednarek, Physica E (Amsterdam) **5**, 185 (2000).
[22] S. T. Chui, Phys. Rev. Lett. **56**, 2395 (1986).
[23] W. Häusler and B. Kramer, Phys. Rev. B **47**, 16353 (1993).
[24] P. A. Maksym and T. Chakraborty, Phys. Rev. Lett. **65**, 108 (1990).
[25] P. Matagne and J. P. Leburton, Phys. Rev. B **65**, 235323 (2002).
[26] W. Kohn, Phys. Rev. **123**, 1242 (1961).
[27] L. Brey, N. F. Johnson, and B. I. Halperin, Phys. Rev. B **40**, 10647 (1989).
[28] F. M. Peeters, Phys. Rev. B **42**, 1486 (1990).
[29] Q. P. Li, K. Karräi, S. K. Yip, S. Das Sarma, and H. D. Drew, Phys. Rev. B **43**, 5151 (1991).
[30] J. F. Dobson, Phys. Rev. Lett. **73**, 2244 (1994).
[31] M. Pi, F. Ancilotto, E. Lipparini, and R. Mayol, Physica E (Amsterdam) **24**, 297 (2004).
[32] T. Sako, P. A. Hervieux, and G. H. F. Diercksen, Phys. Rev. B **74**, 045329 (2006).
[33] J. Adamowski, M. Sobkowicz, B. Szafran, and S. Bednarek, Phys. Rev. B **62**, 4234 (2000).
[34] G. H. F. Diercksen and G. G. Hall, Comput. Phys. **8**, 215 (1994).
[35] M. Wagner, U. Merkt, and A. V. Chaplik, Phys. Rev. B **45**, 1951 (1992).
[36] J. T. Lin and T. F. Jiang, Phys. Rev. B **64**, 195323 (2001).
[37] T. Sako and G. H. F. Diercksen, J. Phys. B **36**, 1681 (2003).
[38] O. Dippel, P. Schmelcher, and L. S. Cederbaum, Phys. Rev. A **49**, 4415 (1994).
[39] W. Becken, P. Schmelcher, and F. K. Diakonos, J. Phys. B **32**, 1557 (1999).
[40] P. S. Drouvelis, P. Schmelcher, and F. K. Diakonos, J. Phys.: Condens. Matter **16**, 3633 (2004).
[41] P. S. Drouvelis, P. Schmelcher, and F. K. Diakonos, Phys. Rev. B **69**, 035333 (2004).
[42] M. Braskén, M. Lindberg, D. Sundholm, and J. Olsen, Phys. Rev. B **61**, 7652 (2000).
[43] S. Corni, M. Braskén, M. Lindberg, J. Olsen, and D. Sundholm, Phys. Rev. B **67**, 085314 (2003).
[44] M. J. Davis, Int. Rev. Phys. Chem. **14**, 15 (1995).
[45] Z.-M. Lu and M. E. Kellmana, J. Chem. Phys. **107**, 1 (1997).
[46] B. Szafran, F. M. Peeters, S. Bednarek, T. Chwiej, and J. Adamowski, Phys. Rev. B **70**, 035401 (2004).
[47] E. Wigner, Phys. Rev. **46**, 1002 (1934).
[48] M. J. Davis and E. J. Heller, J. Chem. Phys. **75**, 246 (1981).
[49] L. Xiao and M. E. Kellman, J. Chem. Phys. **90**, 6086 (1989).
[50] T. Sako and K. Yamanouchi, Chem. Phys. Lett. **264**, 403 (1997).
[51] T. Sako, K. Yamanouchi, and F. Iachello, J. Chem. Phys. **113**, 7292 (2000).
[52] T. Sako, K. Yamanouchi, and F. Iachello, J. Chem. Phys. **114**, 9441 (2001).
[53] T. Sako, K. Yamanouchi, and F. Iachello, J. Chem. Phys. **117**, 1641 (2002).
[54] M. S. Child and R. T. Lawton, Faraday Discuss. Chem. Soc. **71**, 273 (1981).
[55] N. De Leon and E. J. Heller, Phys. Rev. A **30**, 5 (1984).